^{18}F-FDG PET and CT/MRI in Oral Cavity Squamous Cell Carcinoma: A Prospective Study of 124 Patients with Histologic Correlation

Shu-Hang Ng, MD[1]; Tzu-Chen Yen, MD, PhD[2]; Chun-Ta Liao, MD[3]; Joseph Tung-Chieh Chang, MD, MSc[4]; Sheng-Chieh Chan, MD[2]; Sheung-Fat Ko, MD[1]; Hung-Ming Wang, MD[5]; and Ho-Fai Wong, MD[1]

[1]Department of Diagnostic Radiology, Chang Gung Memorial Hospital and Chang Gung University, Taiwan; [2]Department of Nuclear Medicine and Animal Imaging Center, Chang Gung Memorial Hospital and Chang Gung University, Taiwan; [3]Department of Otorhinolaryngology, Chang Gung Memorial Hospital and Chang Gung University, Taiwan; [4]Department of Radiation Oncology, Chang Gung Memorial Hospital and Chang Gung University, Taiwan; and [5]Department of Medical Oncology, Chang Gung Memorial Hospital and Chang Gung University, Taiwan

Accurate evaluation of primary tumors and cervical lymph node status of squamous cell carcinoma (SCC) of the oral cavity is important to treatment planning and prognosis prediction. In this prospective study, we evaluated the use of ^{18}F-FDG PET, CT/MRI, and their visual correlation for the identification of primary tumors and cervical nodal metastases of SCC of the oral cavity with histologic correlation. **Methods:** One hundred twenty-four patients with pathologically proven diagnoses of oral cavity SCC underwent ^{18}F-FDG PET and CT/MRI within 2 wk before surgery. We interpreted ^{18}F-FDG PET, CT/MRI, and visually correlated ^{18}F-FDG PET and CT/MRI separately to assess the primary tumors and their regional lymph node status. We recorded lymph node metastases according to the neck level system of imaging-based nodal classification. Histopathologic analysis was used as the gold standard for assessment of the primary tumors and lymph node involvement. We analyzed differences in sensitivity and specificity among the imaging modalities using the McNemar test. The receiver-operating-characteristic (ROC) curve and calculation of the area under the curve were used to evaluate their discriminative power. **Results:** The accuracy of ^{18}F-FDG PET, CT/MRI, and their visual correlation for the identification of primary tumors was 98.4%, 87.1%, and 99.2%, respectively. The sensitivity of ^{18}F-FDG PET for the identification of nodal metastases on a level-by-level basis was 22.1% higher than that of CT/MRI (74.7% vs. 52.6%, $P < 0.001$), whereas the specificity of ^{18}F-FDG PET was 1.5% lower than that of CT/MRI (93.0% vs. 94.5%, $P = 0.345$). The sensitivity and specificity of the visual correlation of ^{18}F-FDG PET and CT/MRI were 3.2% and 1.5% higher than those of ^{18}F-FDG PET alone (77.9% vs. 74.7%, $P = 0.25$; 94.5% vs. 93.0%, $P = 0.18$, respectively). The area under the curve obtained from the ROC curve showed that ^{18}F-FDG PET was significantly superior to CT/MRI for total nodal detection (0.896 vs. 0.801, $P = 0.002$), whereas the visual correlation of ^{18}F-FDG PET and CT/MRI was modestly superior to ^{18}F-FDG PET alone (0.913 vs. 0.896, $P = 0.28$). **Conclusion:** ^{18}F-FDG PET is superior to CT/MRI in the detection of cervical status of oral cavity SCC. The sensitivity of ^{18}F-FDG PET for the detection of cervical nodal metastasis on a level-by-level basis was significantly higher than that of CT/MRI, whereas their specificities appeared to be similar. Visual correlation of ^{18}F-FDG PET and CT/MRI showed a trend of increased diagnostic accuracy over ^{18}F-FDG PET alone but without a statistically significant difference, and its sensitivity was still not high enough to replace pathologic lymph node staging based on neck dissection.

Key Words: ^{18}F-FDG; PET; head and neck neoplasms; cervical lymph nodes

J Nucl Med 2005; 46:1136–1143

Oral cancer is the sixth most common malignancy worldwide. The presence or absence of cervical malignant adenopathy is the most important prognostic indicator for patients with squamous cell carcinoma (SCC) of the head and neck, along with tumor site and size (*1,2*). Current noninvasive staging techniques include clinical examination, CT, and MRI. Criteria used in the interpretation of CT and MRI for staging lymph nodes include the size of the lymph nodes, the existence of central necrosis, and the presence of indistinct nodal margins (*2–5*). The calculated sensitivity of CT and MRI for detecting lymph node metastases ranges from 36% to 94%, respectively, whereas the reported specificity ranges from 50% to 98% (*6*). It is possible to obtain additional staging information via ultrasound-guided biopsy of the nodes, but this may be impractical in some cases because of the large number of nodes in question. At present, neck dissection with histologic examination is the most reliable staging procedure, providing important prognostic information. There is a need for a noninvasive procedure that provides high-quality prognostic information that approaches this gold standard.

^{18}F-FDG PET is a functional imaging technique that provides information about tissue metabolism and has been

Received Jan. 6, 2005; revision accepted Mar. 29, 2005.

For correspondence or reprints contact: Shu-Hang Ng, MD, Department of Diagnostic Radiology, Chang Gung Memorial Hospital, Linkou Medical Center, 5 Fu-Shin St., Kueishan, Taoyuan 333, Taiwan.

E-mail: Shng6@ms25.hinet.net

successfully applied to the evaluation of head and neck cancer. Currently available data from 15 studies (*3,5,7–19*) demonstrate large variations in sensitivity and specificity for ^{18}F-FDG PET in the detection of cervical lymph node metastases in head and neck cancers. These ranged from 67% to 96% for sensitivity and from 82% to 100% for specificity. A review of these studies showed that the majority of the series had small population sizes. Only 4 of 15 series had a patient number of >50, and only 1 series (*17*) had a patient number of >100 ($n = 106$). The methodology for calculating sensitivity and specificity also differed among these studies, with some based on patient numbers, some based on neck sides, and the remainder based on individual node numbers. Evaluation based on node numbers usually gives a more favorable specificity, because neck dissection typically reveals a large number of tumor-free lymph nodes. Another problem is that it may be difficult to accurately estimate the true number of foci on images with several contiguous foci using ^{18}F-FDG PET. On the other hand, if ^{18}F-FDG PET has different results in different sites of the same neck or of the same patient, one cannot accurately define the sensitivity and specificity based on neck sides or patient numbers. For instance, some patients may demonstrate true-positive nodes at one neck level but false-negative nodes at the other levels. Since neck dissection with histologic examination is currently the most reliable staging procedure, and recording of the cervical nodal location on morphologic imaging (CT or MRI) and neck dissection generally adopts the system of neck levels according to the imaging-based nodal classification (*20*), correlation of imaging results with surgical pathology based on neck levels would be more reliable. Therefore, the calculation of the sensitivity and specificity of ^{18}F-FDG PET based on neck levels would be a better method. However, to our knowledge, no previous studies using this criterion have been reported. In addition, it has been shown that the visual correlation of ^{18}F-FDG PET with CT or MRI can have better diagnostic accuracy than ^{18}F-FDG PET alone in the evaluation of lung cancer and nasopharyngeal carcinoma (*21,22*), but the actual usefulness of such combined use in oral cavity SCC is unknown. Therefore, we conducted a prospective study to determine the usefulness of ^{18}F-FDG PET, CT/MRI, and their combined use in the detection of primary tumors and neck lymph node involvement of SCC of the oral cavity.

MATERIALS AND METHODS

Patients

The institutional review board of our hospital approved this study, with written informed consent obtained from all enrolled subjects. A total of 124 patients were prospectively recruited into this study (121 men, 3 women; average age, 50.5 y; age range, 26–82 y). Inclusion criteria comprised a clinical diagnosis of SCC in the oral cavity, no prior treatment to the head or neck region, and patients were scheduled for dissection. The exclusion criterion was patients with known diabetes mellitus with a fasting serum glucose level of ≥200 ng/mL. Among the 124 patients, 52 (41.9%) had tumors originating from the buccal mucosa, 48 (38.8%) from the tongue, 19 (15.3%) from the gum, 3 (2.4%) from the mouth floor, and 2 (1.6%) from the retromolar trigone. Of the 124 patients, 16 (12.9%) had T1 tumor stage, 56 (45.2%) had T2 tumor stage, 19 (15.3%) had T3 tumor stage, and 33 (26.6%) had T4 tumor stage. In these patients, the preoperative evaluation was accomplished using ^{18}F-FDG PET for all patients ($n = 124$) as well as MRI ($n = 82$) and CT ($n = 42$) within 2 wk before surgery.

^{18}F-FDG PET

The Institute of Nuclear Energy Research of Taiwan produced the ^{18}F-FDG used for the PET studies. All ^{18}F-FDG PET scans were acquired with a dedicated PET system (ECAT EXACT HR+; Siemens/CTI), using a 4.5-mm full width at half maximum and a transaxial field of view of 15 cm. All patients abstained from food and drink for 6 h before undergoing PET. After intravenous injection of 370 MBq (10 mCi) of ^{18}F-FDG, the patients were kept at rest in a quiet, dimly lit room for at least 40 min. Talking, walking, or other physical activities were avoided to reduce muscle uptake.

During imaging, patients kept their arms still over their head, aided by a headrest and a holding bar. We obtained transmission scans with ^{68}Ge rod sources. We obtained the emission and transmission scans in an alternating sequence per bed position. Reconstruction of both transmission and emission scans used accelerated maximum-likelihood reconstruction and ordered-subset expectation maximization, which reduces image noise and avoids reconstruction artifacts resulting from filtered backprojection reconstruction of data with low count densities. We viewed maximum-intensity-projection images on a workstation that allowed simultaneous display of coronal, sagittal, and transverse planes as well as a 3-dimensional rotating projection.

CT/MRI

CT was performed with patients in the supine position with contrast axial scans parallel to the ramus of the mandible from the skull base to the supraclavicular fossa with a 5-mm-thick contiguous section. We also obtained contrast coronal scans with a 3-mm-thick contiguous section. The field of view varied between 16 and 18 cm, depending on the size of the patient. In addition to the soft-tissue window settings, we reconstructed all images with bone algorithms.

All patients underwent MRI with a 1.5-T unit (Vision; Siemens) using spin-echo technique before and after injection of gadolinium diethylenetriaminepentaacetic acid (DTPA). We used a head coil to examine the region from the superior margin of the temporal lobe to the level of the hyoid bone. We then used a neck coil to examine the rest of the neck and the supraclavicular fossa. Unenhanced T1-weighted images were acquired in the sagittal and axial planes with a spin-echo 500/20 (repetition time/echo time, in ms) sequence, a 20-cm field of view, and a 192 × 256 matrix. Axial and coronal T2-weighted fat-suppressed fast-spin-echo images (3,000/85 [effective], 16–echo train length) were also obtained. Section thickness was 5 mm without interslice gap in the axial projection and 4 mm without interslice gap in the sagittal and coronal projections. After gadolinium DTPA injection at a dose of 0.1 mmol/kg of body weight, we obtained T1-weighted fat-suppressed axial, sagittal, and coronal sequences sequentially, with parameters similar to those used before the gadolinium DTPA injection.

Image Interpretation and Analysis

For correlative analysis of nodal staging of ^{18}F-FDG PET, CT/MRI, and the histopathologic examination, the neck was divided into levels based on imaging-based nodal classification (*20*). Level I corresponds to the submental and submandibular nodes. Level II contains the upper jugular nodes from the level of the skull base to the hyoid bone. Level III contains the middle jugular nodes from the level of the hyoid bone to the cricoid cartilage. Level IV contains the lower jugular lymph nodes from the level of the cricoid cartilage to the clavicle. Level V contains the spinal accessory nodes situated posterior to the posterior edge of the sternocleidomastoid muscle. The surgical specimens were referenced to this schema in terms of the position of malignant histologic foci or normal lymph nodes.

Three experienced nuclear medicine physicians interpreted the ^{18}F-FDG PET studies individually by visual inspection of the scans in transverse, sagittal, and coronal sections. They had no knowledge of the CT/MRI or clinical findings. They evaluated foci of increased ^{18}F-FDG uptake with reference to the normal tissue and scored the ^{18}F-FDG uptake on a 5-point scale: 0 = no abnormal uptake, 1 = benign, 2 = probably benign, 3 = probably malignant, and 4 = definitely malignant. Both grade 3 and grade 4 were considered to be positive results for tumor involvement. A checklist of the distributions of the primary tumors and their metastatic nodes was recorded accordingly. We resolved any initial differences of opinion by consensus. We did not use standardized uptake values for this study, because these numbers cannot provide meaningful help in discriminating between metastatic and reactive lymph nodes (*10,13,15*).

CT or MRI was interpreted in a blinded fashion by 2 radiologists with experience in this field. Any disagreements were resolved by consensus. The radiologists compiled the same checklist using the same 5-point scale as applied to the ^{18}F-FDG PET images. Nodes were considered metastatic if their shortest axial diameter was ≥11 mm in the jugulodigastric region or ≥10 mm in other cervical regions, if central necrosis or irregular borders were present, or if there was a cluster of 3 or more lymph nodes of borderline size.

To determine the accuracy of visual correlation of ^{18}F-FDG PET and CT/MRI in evaluation of oral cavity SCC, the nuclear medicine physicians and the radiologists met weekly to view the ^{18}F-FDG PET and CT/MR images side-by-side. The same checklist was complied together and solved any discordance by consensus.

The sensitivity, specificity, accuracy, positive predictive value, and negative predictive value of ^{18}F-FDG PET and CT/MRI were calculated based on neck levels. In subcategorizing the nodes by level, the numbers per level were reduced and the confidence intervals in each level thereby would become wider. To compensate for this problem and to get more statistically significant data, we grouped all levels together for our results. Differences in cumulative sensitivity and specificity between the imaging modalities were tested for statistical significance using the McNemar test. In addition, to compare the diagnostic accuracy of the imaging procedures, a receiver-operating- characteristic (ROC) curve analysis using the method of Metz (*23*) was performed, and the area under the ROC curve (area under the curve) was calculated for each modality and compared statistically.

Surgical Procedure or Histology

Neck dissection was planned by our head and neck surgical team based on the clinical and imaging findings. Supraomohyoid neck dissection (levels I–III) was performed in patients with negative neck or a single positive node in the upper neck. Extended supraomohyoid neck dissection (levels I–IV) or modified radical neck dissection (levels I–V) was performed in those patients with >1 involved node or extracapsular nodal spread, depending on the extent of the cervical adenopathy. Bilateral neck dissection was performed in patients with the primary tumor crossing the midline or with probably metastatic nodes in the contralateral neck. The operative surgeon labeled primary tumor and neck dissection specimens in such a way that one could reference the schema used in the interpretation of the ^{18}F-FDG PET and CT/MRI studies. Lymph nodes and tumors were dissected from the specimens and stained with hematoxylin and eosin for histologic analysis. Serial histologic sections were used. An experienced anatomic pathologist examined the specimens and recorded the size of tumor deposition within the affected nodes. In cases with equivocal findings for tumor deposition, cytokeratin stain was performed. We compared the results of preoperative imaging examinations with the results of corresponding histopathologic examinations.

RESULTS

All of our 124 patients underwent primary tumor resection and neck dissection. There were 5 diabetic patients in this series. They were enrolled because their serum sugar was controlled to <200 ng/mL with medication at the time they underwent ^{18}F-FDG PET examination. In the 493 neck levels (6,475 nodes) resected in these 124 patients, 95 neck levels (154 nodes) contained metastatic disease in 53 patients. Twenty-seven (51%) of the 53 patients had >1 neck level involved histologically, such that the mean number of levels involved per patient was 1.8. Grossly, the mean size ± SD of these 154 affected nodes was 13.4 ± 6.2 mm. Microscopically, the mean size and the mean percentage of tumor deposit within the affected nodes were 8.9 ± 6.8 mm and 63.7% ± 29.5%, respectively.

Primary Tumors

^{18}F-FDG PET correctly identified the primary tumor in 122 of the 124 patients. There were only 2 false-negative study results for the detection of the primary tumors (accuracy for the detection of primary tumors): one was a superficial tumor that occurred in the left lateral tongue with histopathologic dimensions of 1.0 × 1.0 × 0.1 cm; the other tumor was a mouth floor SCC, which was misinterpreted as a tongue SCC on the ^{18}F-FDG PET scan. In contrast, CT/MRI correctly identified 108 of the 124 oral cavity SCCs (accuracy, 87.1%). An artifact caused by a metallic dental prosthesis obscured the site of primary tumors in 7 of the 16 false-negative CT/MRI results. The other 9 lesions were small tumors with a T-stage of T1 (i.e., <2 cm in their greatest dimension). Of the 16 primary tumors not identifiable with CT/MRI, ^{18}F-FDG PET detected 15 (Fig. 1). The visually correlated ^{18}F-FDG PET and CT/MRI correctly identified 123 tumors with an accuracy of 99.2%.

Metastatic Neck Disease

The results of CT/MRI, ^{18}F-FDG PET, and their combination in identifying metastatic neck nodes of these 124

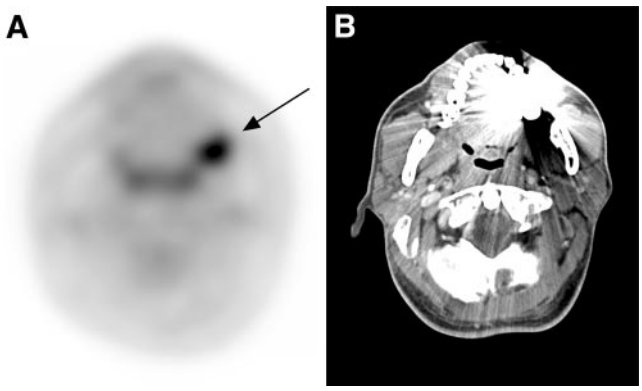

FIGURE 1. ^{18}F-FDG PET clearly demonstrates left retromolar trigone SCC (arrow) (A), but it is obscured by dental artifact on CT (B).

patients with oral cavity SCC are listed in Table 1. On a level-by-level basis, ^{18}F-FDG PET detected disease accurately in 441 of 493 neck levels (89.4%), being truly positive in 71 levels and truly negative in 370 levels. CT/MRI detected levels of metastatic disease accurately in 426 of 493 neck levels (86.4%), being truly positive in 50 levels and truly negative in 376 levels. The sensitivity of ^{18}F-FDG PET was 22.1% higher than that of CT/MRI (74.7% vs. 52.6%, $P < 0.001$), whereas the specificity of ^{18}F-FDG PET was 1.5% lower than that of CT/MRI (93.0% vs. 94.5%, $P = 0.345$). The sensitivity and specificity of the visual correlation of ^{18}F-FDG PET and CT/MRI were 3.2% and 1.5% higher than those of ^{18}F-FDG PET alone (77.9% vs. 74.7%, $P = 0.25$; 94.5% vs. 93.0%, $P = 0.18$, respectively). The area under the curve obtained from the ROC curve showed that ^{18}F-FDG PET was significantly superior to CT/MRI for total nodal detection (0.896 vs. 0.801, $P = 0.002$), whereas the visual correlation of ^{18}F-FDG PET and CT/MRI was slightly superior to ^{18}F-FDG PET alone without statistical significance (0.913 vs. 0.896, $P = 0.28$) (Fig. 2).

^{18}F-FDG PET had positive findings in 99 neck levels, of which 71 were true-positive and 28 were false-positive. Among the 28 false-positive ^{18}F-FDG PET results, 25 were caused by reactive or inflammatory nodes. The other 3 were caused by misinterpretation of submandibular gland lesions as level I nodal metastases (Fig. 3), including direct tumor invasion ($n = 2$) and sialoadenitis ($n = 1$). Of these 28 ^{18}F-FDG PET false-positive neck levels, CT/MRI showed true-negative findings in 10 levels but false-positive findings in the other 18 levels.

Conversely, ^{18}F-FDG PET had negative findings in 394 neck levels, of which 370 were true-negative and 24 were false-negative. Pathologically, 37 metastatic nodes were

TABLE 1
Results of ^{18}F-FDG PET, CT/MRI, and Their Visual Correlation in 124 Patients with Oral Cavity SCC

Neck level	FN	TP	TN	FP	Sensitivity (%)	Specificity (%)	Accuracy (%)	PPV (%)	NPV (%)
Level I									
CT/MRI	21	29	93	8	58.0 (43.2–71.8)	92.1 (85.0–96.5)	80.8 (73.6–86.7)	78.4 (61.8–90.2)	81.6 (73.2–88.2)
^{18}F-FDG PET	10	40	91	10	80.0 (66.3–90.0)	90.1 (82.5–95.1)	86.8 (80.3–91.7)	80.0 (66.3–90.0)	90.1 (82.5–95.1)
CT/MRI + ^{18}F-FDG PET	9	41	94	7	82.0 (68.6–91.4)	93.1 (86.2–97.2)	89.4 (83.4–93.8)	85.4 (72.2–93.9)	91.3 (84.1–95.9)
Level II									
CT/MRI	11	16	111	12	59.3 (38.8–77.6)	90.2 (83.6–94.9)	84.7 (77.9–90.0)	57.1 (37.2–75.5)	91.0 (84.4–95.4)
^{18}F-FDG PET	5	22	109	14	81.5 (61.9–93.7)	88.6 (81.6–93.6)	87.3 (80.9–92.2)	61.1 (43.5–76.9)	95.6 (90.1–98.6)
CT/MRI + ^{18}F-FDG PET	4	23	110	13	85.2 (66.3–95.8)	89.4 (82.6–94.3)	88.7 (82.5–93.3)	63.9 (46.2–79.2)	96.5 (91.3–99.0)
Level III									
CT/MRI	9	5	133	2	35.7 (12.8–64.9)	98.5 (94.8–99.8)	92.6 (87.2–96.3)	71.4 (29.0–96.3)	93.7 (88.3–97.1)
^{18}F-FDG PET	7	7	131	4	50.0 (23.0–77.0)	97.0 (92.6–99.2)	92.6 (87.2–96.3)	63.6 (30.8–89.1)	94.9 (89.8–97.9)
CT/MRI + ^{18}F-FDG PET	6	8	133	2	57.1 (28.9–82.3)	98.5 (94.8–99.8)	94.6 (89.7–97.7)	80.0 (44.4–97.5)	95.7 (90.8–98.4)
Level IV									
CT/MRI	4	0	21	0	0	100	84.0 (63.9–95.5)	—	84.0 (63.9–95.5)
^{18}F-FDG PET	2	2	21	0	50.0 (6.8–93.2)	100	92.0 (74.0–99.0)	100	91.3 (72.0–98.9)
CT/MRI + ^{18}F-FDG PET	2	2	21	0	50.0 (6.8–93.2)	100	92.0 (74.0–99.0)	100	91.3 (72.0–98.9)
Level V									
CT/MRI	0	0	18	0	—	100	100	—	100
^{18}F-FDG PET	0	0	18	0	—	100	100	—	100
CT/MRI + ^{18}F-FDG PET	0	0	18	0	—	100	100	—	100
Total									
CT/MRI	45	50	376	22	52.6 (42.1–63.0)	94.5 (91.8–96.5)	86.4 (83.1–89.3)	69.4 (57.5–79.8)	89.3 (86.0–92.1)
^{18}F-FDG PET	24	71	370	28	74.7 (64.8–83.1)	93.0 (90.0–95.3)	89.5 (86.4–92.0)	71.7 (61.8–80.3)	93.9 (91.1–96.1)
CT/MRI + ^{18}F-FDG PET	21	74	376	22	77.9 (68.2–85.8)	94.5 (91.8–96.5)	91.3 (88.4–93.6)	77.1 (67.4–85.0)	94.7 (92.0–96.7)

FN = false-negative; TP = true-positive; TN = true-negative; FP = false-positive; PPV = positive predictive value; NPV = negative predictive value.

Ranges in parentheses are 95% confidence intervals.

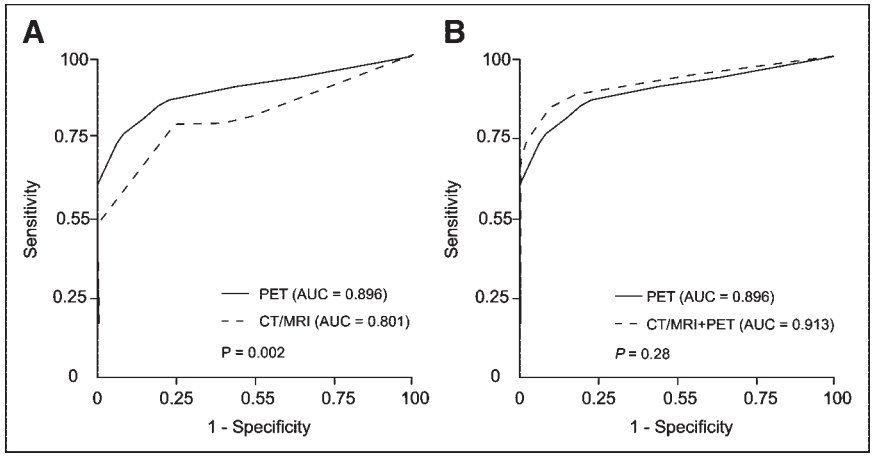

FIGURE 2. ROC curve and area under the curve (AUC) show that discriminative power of ^{18}F-FDG PET is significantly superior to that of CT/MRI for cervical nodal detection (AUC, 0.896 vs. 0.801, $P = 0.002$) (A), whereas visual correlation of ^{18}F-FDG PET and CT/MRI is marginally superior to ^{18}F-FDG PET alone (AUC, 0.913 vs. 0.896, $P = 0.28$) (B).

found among these 24 ^{18}F-FDG PET false-negative neck levels. In comparison with the ^{18}F-FDG PET true-positive nodes, the mean nodal size of the ^{18}F-FDG PET false-negative nodes was 19% smaller (11.4 ± 4.9 mm vs. 14.1 ± 6.5 mm, $P = 0.061$), whereas the average size of intranodal tumor deposits was 46% smaller (5.5 ± 4.7 mm vs. 10.2 ± 7.1 mm, $P = 0.005$). The median size of the intranodal tumor extent in the ^{18}F-FDG PET false-negative nodes was also considerably lower than that in the ^{18}F-FDG PET true-positive nodes (4.3 vs. 9 mm). Of the 24 neck levels where ^{18}F-FDG PET was false-negative for metastatic neck disease, CT/MRI showed true-positive findings in only 3 levels (12.5%), in which all harbored nodes with central necrosis (Fig. 4).

CT/MRI had positive findings in 72 neck levels, of which 50 were true-positive and 22 were false-positive. Nodal size accounted for the majority of the positive CT/MRI findings, whereas the more specific signs of metastasis (central necrosis or irregular border) accounted for about one third. Central nodal necrosis was seen in 12 levels, irregular nodal border indicating extracapsular spread was seen in 8 levels, and both were seen in 4 levels. All such 16 cervical levels with nodal central necrosis were true-positive for metastasis, whereas 10 of the 12 levels with irregular nodal border were true-positive. Of 22 false-positive levels of CT/MRI, ^{18}F-FDG PET showed true-negative findings in 11 levels. On the other hand, CT/MRI failed to identify metastatic neck disease in 45 levels. Among these 45 levels, ^{18}F-FDG PET detected 24 (Fig. 5), whereas the other 21 diseased levels were also negative on ^{18}F-FDG PET.

DISCUSSION

Head and neck carcinomas constitute approximately 5% of all malignancies worldwide, and the incidence of tumors of the head and neck is increasing. The great majority of these tumors are SCC, which accounts for about 95% of all head and neck tumors (*24,25*). There is an increased frequency of carcinoma in smokers and in patients with a history of excessive alcohol use. Researchers have also noted the association of SCC of the oral mucosa and the chewing of betel quid (*26*). In our series, the tumor with the highest incidence was SCC of the buccal mucosa, compatible with the high prevalence of betel quid chewing in

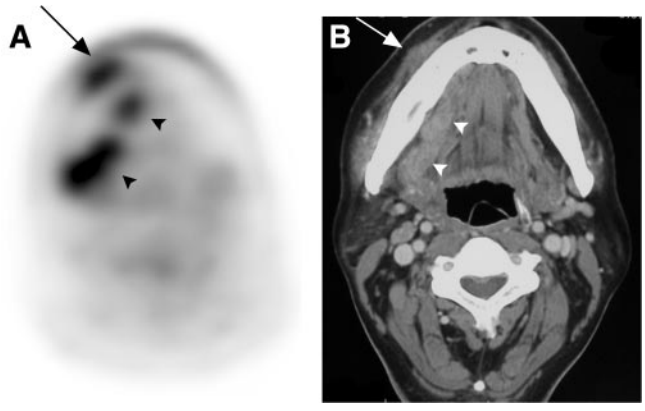

FIGURE 3. Right gum SCC (arrows) with submandibular gland invasion (arrowheads) is falsely interpreted as level I metastatic nodes on ^{18}F-FDG PET (A) but is well demonstrated on CT (B).

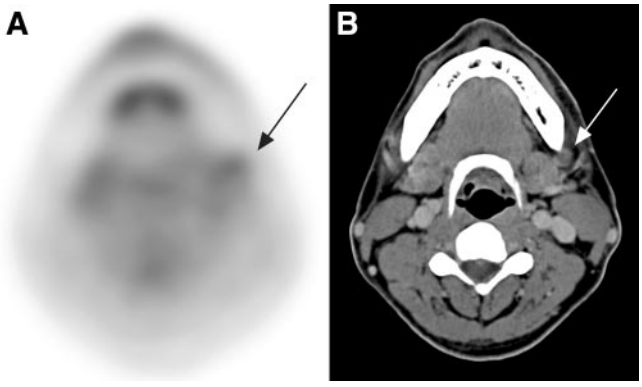

FIGURE 4. ^{18}F-FDG PET falsely suggests benign left level I node (arrow) due to low ^{18}F-FDG uptake (score 1) (A). CT shows central necrosis in corresponding node (arrow), indicating malignancy (B). Resection of this node revealed presence of metastatic SCC.

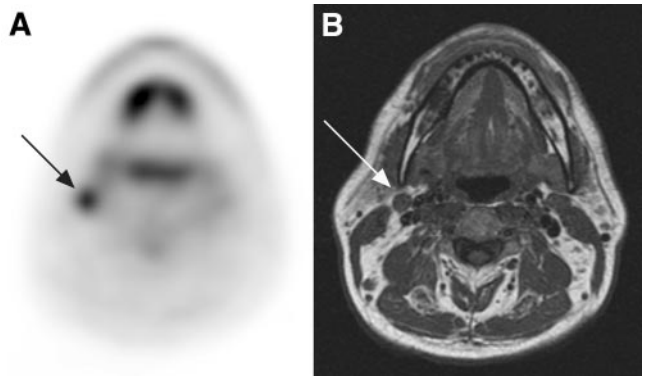

FIGURE 5. (A) ^{18}F-FDG PET shows true-positive finding in right neck level II (arrow). (B) T1-weighted MRI shows small right level II node (arrow), suggesting a benign node by size. Histopathologic examination revealed that this node harbored metastatic SCC.

patients with oral cavity SCC in our country. Although a considerable number of studies of ^{18}F-FDG PET in the preoperative evaluation of head and neck cancer has been previously published (*3,5,7–19*), the majority of such publications had small patient populations. Our study enrolled 124 patients with newly diagnosed oral cavity SCC and, to the best of our knowledge, it would appear to be the largest series yet reported.

The present management of head and neck cancer mainly consists of resection of the primary tumor, which may be coupled with neck surgery or subsequent radiotherapy. It is evident from the literature (*12,15,18*) that ^{18}F-FDG PET is very sensitive for detecting primary tumors in the oral cavity, and our data further support these findings. Our data demonstrate an accuracy of 98.4% for ^{18}F-FDG PET in the detection of known primary tumors and of 85.1% for CT/MRI in this setting. ^{18}F-FDG PET missed only 1 small tongue SCC and misinterpreted a mouth floor SCC as a tongue SCC. However, ^{18}F-FDG PET does not provide the detailed information necessary for surgical planning of primary tumor resection, such as information regarding the depth of penetration and any change in neighboring structures. CT or MRI, by virtue of their better anatomic resolution, remain the methods of choice for evaluation of the primary tumor with reliable T-staging in 80%–90% of cases (*25,27*). Nevertheless, ^{18}F-FDG PET appears to be helpful for the identification of primary oral cavity tumors not seen in morphologic imaging modalities, particularly those obscured by dental artifacts.

The critical determinant of the utility of an imaging modality for oral cavity SCC is its ability to detect the presence or absence of metastatic neck disease. This information has the potential to alter the treatment plan and patient morbidity. At present, neck dissection with histologic examination is the most reliable staging procedure that provides important prognostic information, but it does involve the resection of a large amount of nondiseased tissue from the neck. In our study with 493 neck levels dissected, only 95 (19.3%) contained metastatic disease. In accordance with most published results (*3,7,9,11–16,19*), our study showed that ^{18}F-FDG PET was significantly superior to CT/MRI for identifying metastatic neck lesions (area under the curve, 0.911 vs. 0.794; $P = 0.0026$), with a significantly higher sensitivity (74.7% vs. 52.6%, $P < 0.001$). ^{18}F-FDG PET disclosed metastatic lesions in approximately half of the morphologically benign nodes; however, the sensitivity of ^{18}F-FDG PET was just 74.7%, and 24 of 95 pathologically positive neck levels (25%) were false-negative on ^{18}F-FDG PET. Therefore, ^{18}F-FDG PET does not provide sufficient information to limit surgical dissection or radiotherapy porta in the neck.

In affected lymph nodes, the size of the node and the size of the intranodal tumor deposits appear to vary widely. As seen in our series, the mean percentage of tumor deposit within the affected nodes was 69.31% ± 27.7%. Previous studies (*17,28*) showed that the extent of the intranodal tumor deposit is a more limiting determinate than the nodal size. Wooglar et al. (*29*) have reported that micrometastases were found as the only metastases in 28% of clinically N0 side of the neck. Crippa et al. (*28*) subjected 38 patients to preoperative ^{18}F-FDG PET and correlated the sensitivities for detection of nodal metastases with the nodal deposit diameter; they found a nonsignificant correlation between the size of a lymph node metastasis and the ability to detect it (*17*). On the contrary, ^{18}F-FDG PET has technical resolution limitations of about 5 mm and, thus, is not likely to be able to detect small-volume disease, contributing to false-negative results. Our study showed that the mean intranodal tumor extent of ^{18}F-FDG PET false-negative nodes was half that of ^{18}F-FDG PET true-positive nodes (5.5 vs. 10.2 mm, $P = 0.005$), whereas the mean size of false-negative nodes was just slightly smaller than that of true-positive nodes (11.4 vs. 14.1 mm, $P = 0.061$). These results support the notion that intranodal tumor deposits play a determinate role in the sensitivity of ^{18}F-FDG PET and suggest that ^{18}F-FDG PET would be likely to miss those nodes with a mean tumor deposit of about 5.5 mm or less.

^{18}F-FDG PET has been reported to have a higher specificity than CT/MRI in detecting cervical nodal disease in most of the published literature (*3,7,9,11–18*). Only 2 articles (*10,19*) reported that ^{18}F-FDG PET had a lower specificity. Our study showed the specificity of ^{18}F-FDG PET was just marginally lower than that of CT/MRI (93.0% vs. 94.5%, $P = 0.345$). False-positive ^{18}F-FDG PET findings were mainly due to its inherent inability to discriminate inflammatory processes from tumor infiltration since high-level metabolic changes occur in both instances. Spatial inaccuracy contributed to a portion of the false-positive results. The relatively poor spatial resolution of ^{18}F-FDG PET led to misinterpretation of submandibular gland lesions as level I metastatic adenopathy in 3 of our 28 (10.8%) false-positive neck levels.

Nodal central necrosis demonstrated on CT/MRI carries a very high specificity for nodal metastasis; however, the

occurrence of such necrosis is not high. Nodal necrosis associates with the loss of viable tumor cells and may cause false-negative findings on ^{18}F-FDG PET when the node is largely necrotic because few viable cells are available to accumulate the tracer (*14*). Our series demonstrated gross nodal necrosis in 16 of our 95 positive neck levels (16.8%) on CT/MRI, and these were not always associated with false-negative findings on ^{18}F-FDG PET. Of the 16 necrotic nodal groups, only 3 were responsible for the false-negative results on ^{18}F-FDG PET, whereas the remaining 13 still exhibited positive ^{18}F-FDG uptake with nodular or rim configurations.

Some studies have reported that the visual correlation of ^{18}F-FDG PET with CT/MRI has better diagnostic accuracy than ^{18}F-FDG PET alone (*21,22,30*). In this large series of oral cavity SCC, we also evaluated neck levels for nodal metastasis with meticulous side-by-side visual correlation of ^{18}F-FDG PET and CT/MRI. Combined use increased the sensitivity by 3.2% over ^{18}F-FDG PET alone (77.9% vs. 74.7%, $P = 0.25$). This increment was due to correction of 3 false-negative ^{18}F-FDG PET results attributed largely to necrotic nodes. The specificity of the combined use also increased by 1.5% over ^{18}F-FDG PET alone (94.5% vs. 93.0%, $P = 0.18$), attributed to the correction of false-positive ^{18}F-FDG PET results due to spatial inaccuracy. The area under the curve obtained from the ROC curve showed that the combined use had a slightly higher diagnostic accuracy than ^{18}F-FDG PET alone (0.913 vs. 0.896, $P = 0.28$). However, this improvement is not statistically significant, presumably due to the fact that visual correlation of ^{18}F-FDG PET and CT/MRI could not alleviate the main diagnostic difficulties inherent in ^{18}F-FDG PET and CT/MRI, including some false-negative findings due to small intranodal tumor deposits and some false-positive findings due to inflammatory nodal hyperplasia. In our study, the sensitivity of the visual correlation of ^{18}F-FDG PET and CT/MRI was 77.9%, and 21 of 95 pathologic positive neck levels (22%) were false-negative on this methodology. Therefore, its sensitivity was not high enough to replace pathologic lymph node staging of oral cavity SCC based on neck dissection.

Since imaging was used in the planning of neck dissection, some verification bias could have been introduced because the extent of neck dissection would vary with imaging findings. For instance, contralateral neck dissection was performed because imaging showed positive findings for contralateral nodal metastasis. However, this approach represents realistic daily clinical practice and, hence, such bias was essentially unavoidable.

Coregistration of ^{18}F-FDG PET images with CT or MRI scans of the same patient can be performed by a computer algorithm to combine the images in one display using either anatomic landmarks or an automatic algorithm based on matching the pattern of signals from individual voxels. However, in clinical practice, it is time-consuming and somewhat difficult to accomplish due to variations in neck position (*31*). Recently, integrated PET/CT with simultaneous, coregistered anatomic and functional imaging has been introduced. It is more accurate than PET alone in the detection and anatomic localization of head and neck cancer (*31*). Such hybrid machines have also been reported to have significantly better diagnostic accuracy than visual correlation of PET and CT in the evaluation of lung cancer (*32*). If available, it would be worthwhile to test whether this novel technique provides such significant advantages for oral cavity SCC.

CONCLUSION

In this large series of oral cavity SCC, ^{18}F-FDG PET proved to be significantly superior to CT/MRI in the detection of cervical lymph node status of oral cavity SCC. The sensitivity of ^{18}F-FDG PET for the detection of cervical nodal metastasis on a level-by-level basis was significantly higher than that of CT/MRI, whereas their specificities appeared to be quite similar. Visual correlation of ^{18}F-FDG PET and CT/MRI showed a trend of increased diagnostic accuracy over ^{18}F-FDG PET alone, but without a statistically significant difference, and its sensitivity was still not high enough to replace pathologic lymph node staging based on neck dissection.

ACKNOWLEDGMENTS

We gratefully acknowledge grants from the National Science Council–Taiwan (NSC 93-2314-B-182A-106) and from the Chang Gung Memorial Hospital (CMRPG-32034 and CMRPG-32039).

REFERENCES

1. Brown AE, Langdon JD. Management of oral cancer. *Ann R Coll Surg Engl.* 1995;77:404–408.
2. Snow GB, Patel P, Leemans CR, Tiwari R. Management of cervical lymph nodes in patients with head and neck cancer. *Eur Arch Otorhinolaryngol.* 1992;249:187–194.
3. Bailet JW, Abemayor E, Jabour BA, et al. Positron emission tomography: a new, precise imaging modality for detection of primary head and neck tumors and assessment of cervical adenopathy. *Laryngoscope.* 1992;102:281–288.
4. Don DM, Anzai Y, Lufkin RB, et al. Evaluation of cervical lymph node metastases in squamous cell carcinoma of the head and neck. *Laryngoscope.* 1995;105:669–674.
5. McGuirt WF, Williams DW III, Keyes JW Jr, et al. A comparative diagnostic study of head and neck nodal metastases using positron emission tomography. *Laryngoscope.* 1995;105:373–375.
6. Conti PS, Lilien DL, Hawley K, et al. PET and [F-18]-FDG in oncology: a clinical update. *Nucl Med Biol.* 1996;23:717–735.
7. Jabour BA, Choi Y, Hoh CK, et al. Extracranial head and neck: PET imaging with 2-[F-18]fluro-2-deoxy-D-glucose and MR imaging correlation. *Radiology.* 1993;186:27–35.
8. Rege S, Maass A, Chaiken L, et al. Use of positron emission tomography with fluorodeoxyglucose in patients with extracranial head and neck cancers. *Cancer.* 1994;73:3047–3058.
9. Laubenbacher C, Saumweber D, Wagner-Manslau C, et al. Comparison of fluorine-18-fluorodeoxyglucose PET, MRI, and endoscopy for staging head and neck squamous cell carcinomas. *J Nucl Med.* 1995;36:1747–1757.
10. Braams JW, Pruim J, Freling NJM, et al. Detection of lymph node metastases of squamous cell cancer of the head and neck with FDG PET and MRI. *J Nucl Med.* 1995;36:211–216.
11. Benchaou M, Lehman W, Slosman DO, et al. The role of FDG PET in the pre-operative assessment of N staging in head and neck cancer. *Acta Otolaryngol.* 1996;116:332–335.

12. Wong WL, Chevretton EB, McGurk M, et al. A prospective study of PET-FDG imaging for the assessment of head and neck squamous cell carcinoma. *Clin Otolaryngol.* 1997;22:209–214.
13. Adams S, Baum RP, Stuchensen T, et al. Prospective comparison of ^{18}F-FDG PET with conventional imaging modalities (CT, MRI, US) in lymph node staging of head and neck cancer. *Eur J Nucl Med.* 1998;25:1255–1260.
14. Kau RJ, Alexiou C, Laubenbacher C, Werner M, Schwaiger M, Arnold W. Lymph node detection of head and neck squamous cell carcinomas by positron emission tomography with fluorodeoxyglucose F18 in a routine clinical setting. *Arch Otolaryngol Head Neck Surg.* 1999;125:1322–1328.
15. Nowak B, Martino ED, Janicke S, et al. Diagnostic evaluation of malignant head and neck cancer by F-18-FDG PET compared with CT/MRI. *Nuklearmedizin.* 1999;38:312–318.
16. Stokkel MPM, ten Broek FW, Hordijk GJ, et al. Preoperative evaluation of patients with primary head and neck cancer using dual-head 18 fluorodeoxyglucose positron emission tomography. *Ann Surg.* 2000;231:229–234.
17. Stuckensen T, Kovacs AF, Adams S, Baum RP. Staging of the neck in patients with oral cavity squamous cell carcinomas: a prospective comparison of PET, ultrasound, CT and MRI. *J Craniomaxillofac Surg.* 2000;28:319–324.
18. Hannah A, Scott AM, Tochon-Danguy H. Evaluation of ^{18}F-fluorodeoxyglucose positron emission tomography and computed tomography with histopathologic correlation in the initial staging of head and neck cancer. *Ann Surg.* 2002;2:208–217.
19. Hlawitschka M, Neise E, Bredow J, et al. FDG PET in the pretherapeutic evaluation of primary squamous cell carcinoma of the oral cavity and the involvement of cervical lymph nodes. *Mol Imaging Biol.* 2002;4:91–98.
20. Som PM, Curtin HD, Mancuso AA. Imaging-based nodal classification for evaluation of neck metastatic adenopathy. *AJR.* 2000;174:837–844.
21. Vansteenkiste JF, Stroobants SG, Dupont PJ, et al. FDG PET scan in potentially operable non-small cell lung cancer: do anatometabolic PET-CT fusion images improve the localisation of regional lymph node metastases? The Leuven Lung Cancer Group. *Eur J Nucl Med Mol Imaging.* 1998;25:1495–1501.
22. Ng SH, Chang JTC, Chan SC, et al. Nodal metastases of nasopharyngeal carcinoma: patterns of disease on MRI and FDG PET. *Eur J Nucl Med Mol Imaging.* 2004;31:1073–1080.
23. Metz CE. ROC methodology in radiology imaging. *Invest Radiol.* 1986;21:720–733.
24. Steiner W. Early detection of cancer in the upper aerodigestive tract. Part I. *HNO.* 1993;41:360–367.
25. Steinkamp HJ, Maurer J, Heim T, et al. Magnetic resonance tomography and computerized tomography in tumor staging of mouth and oropharyngeal cancer. *HNO.* 1993;41:519–525.
26. Chong KM. Betel nut chewing and mouth cancer in Taiwan: observation of the oral mucosa in the betel nut chewers. *J Formos Med Assoc.* 1996;65:79–85.
27. Glazer H, Niemyer JH, Blafer DM. Neck neoplasms: MRI imaging—Part I: initial evaluation. *Radiology.* 1986;160:343–348.
28. Crippa F, Leutner M, Belli F, et al. Which kinds of lymph node metastases can FDG-PET detect? a clinical study in melanoma. *J Nucl Med.* 2004;41:1491–1494.
29. Woolgar JA, Vaughan ED, Scott J, et al., Pathological findings in clinically false-negative and false-positive neck dissections for oral carcinoma. *Ann R Coll Surg Engl.* 1994;76:237–244.
30. Yang M, Martin DR, Karabulut N, Frick MP. Comparison of MR and PET imaging for the evaluation of liver metastases. *J Magn Reson Imaging.* 2003;17:343–349.
31. Schoder H, Yeung HW, Gonen M, Kraus D, Larson SM. Head and neck cancer: clinical usefulness and accuracy of PET/CT image fusion. *Radiology.* 2004;231:65–72.
32. Lardinois D, Brack T, Gaspert A, et al. Staging of non-small-cell lung cancer with integrated positron-emission tomography and computed tomography. *N Engl J Med.* 2003;348:2500–2507.

JNM The Journal of NUCLEAR MEDICINE

^{18}F-FDG PET and CT/MRI in Oral Cavity Squamous Cell Carcinoma: A Prospective Study of 124 Patients with Histologic Correlation

Shu-Hang Ng, Tzu-Chen Yen, Chun-Ta Liao, Joseph Tung-Chieh Chang, Sheng-Chieh Chan, Sheung-Fat Ko, Hung-Ming Wang and Ho-Fai Wong

J Nucl Med. 2005;46:1136-1143.

The Journal of Nuclear Medicine is published monthly.
SNMMI | Society of Nuclear Medicine and Molecular Imaging
1850 Samuel Morse Drive, Reston, VA 20190.
(Print ISSN: 0161-5505, Online ISSN: 2159-662X)

SNMMI SOCIETY OF NUCLEAR MEDICINE AND MOLECULAR IMAGING